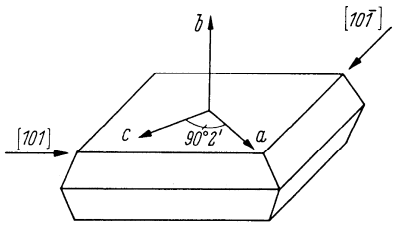

Fig. 48A-2-001. $K_4Fe(CN)_6 \cdot 3H_2O$. Crystal form [60Wak1].

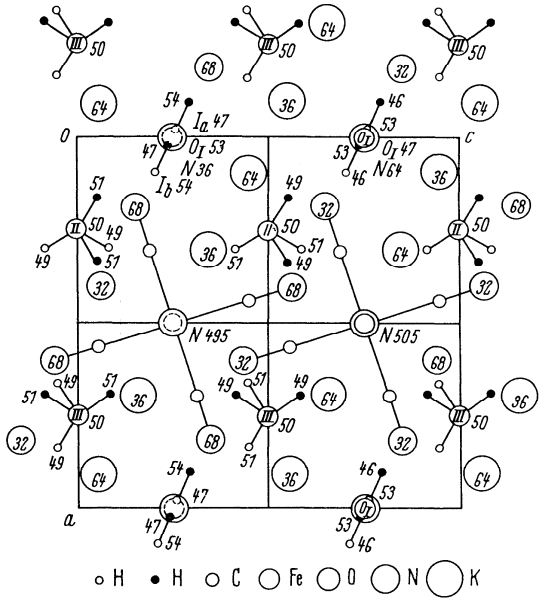

Fig. 48A-2-002. $K_4Fe(CN)_6 \cdot 3H_2O$. Crystal structure [(010) projection] in phase II [64Kir]. The figures indicate the *y* parameters. Only the water layer at *b*/2 and its neighbours are included. There are two kinds of H_2O molecules in phase I; $2H_2O$ at 8(f) and H_2O at 4(e). In phase II a unit cell contains three kinds, the two at 8(f) becoming not equivalent (H_2O–I, –II, –III). H_{Ia} and H_{Ib} are two possible configurations with equal probability, provided that the positions of the heavy atoms are the same in both phases. They are indicated by open and full circles.

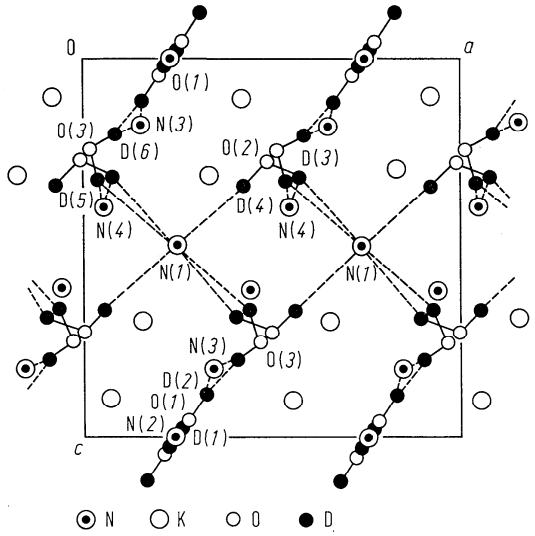

Fig. 48A-2-003. $K_4Fe(CN)_6 \cdot 3D_2O$. Crystal structure in phase I [70Tay]. Atoms near $y = 0.5$ are projected on (010). Disordered water molecules and possible hydrogen bonds are shown.

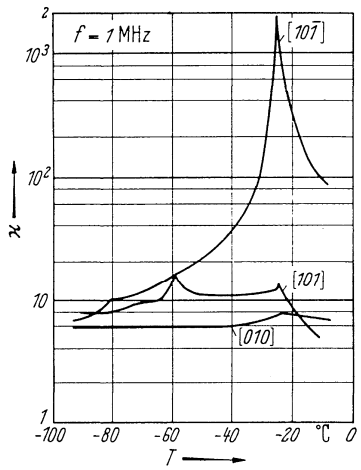

Fig. 48A-2-004. $K_4Fe(CN)_6 \cdot 3H_2O$. $\varkappa$ vs. T [60Wak1].

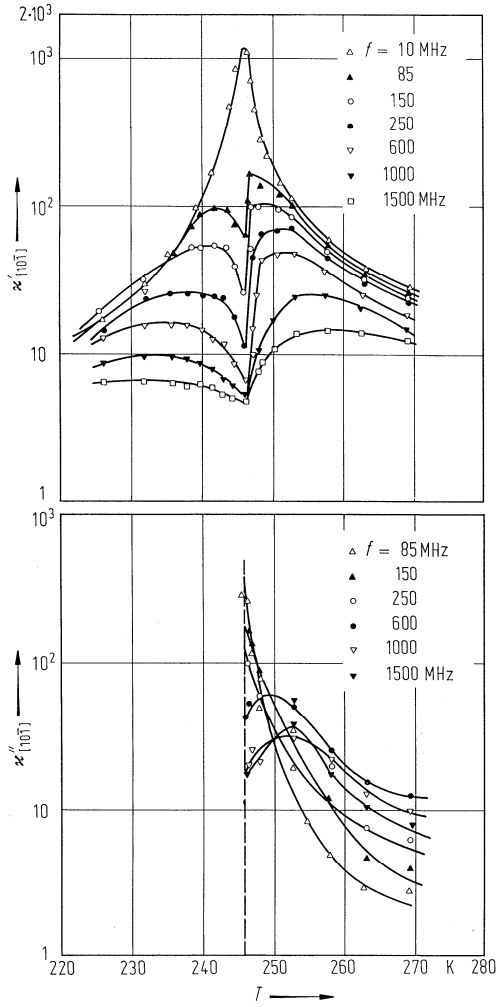

Fig. 48A-2-005. $K_4Fe(CN)_6 \cdot 3H_2O$. $\kappa'_{[10\bar{1}]}$ and $\kappa''_{[10\bar{1}]}$ vs. T [80Kol]. Parameter: f.

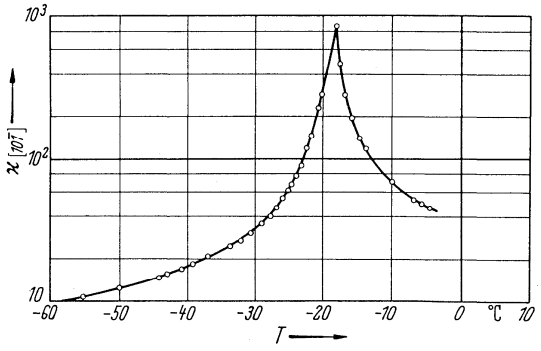

Fig. 48A-2-006. $K_4Fe(CN)_6 \cdot 3D_2O$. $\kappa_{[10\bar{1}]}$ vs. T [60Wak2].

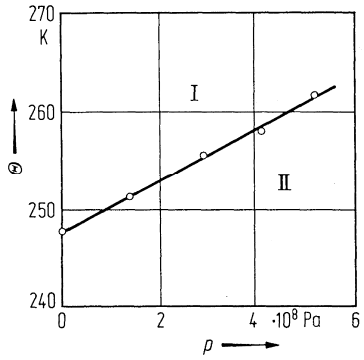

Fig. 48A-2-007. $K_4Fe(CN)_6 \cdot 3H_2O$. Θ vs. p [69Kra]. p: hydrostatic pressure.

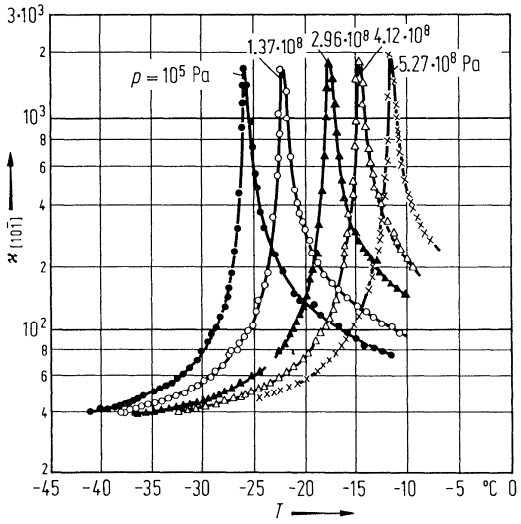

Fig. 48A-2-008. $K_4Fe(CN)_6 \cdot 3H_2O$. $\kappa_{[10\bar{1}]}$ vs. T [69Kra]. Parameter: p.

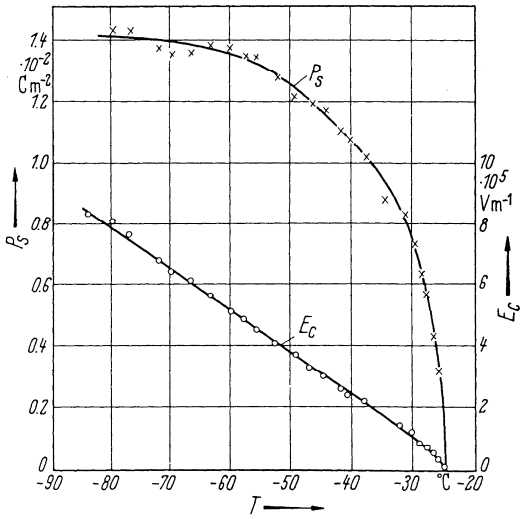

Fig. 48A-2-009. $K_4Fe(CN)_6 \cdot 3H_2O$. P_s, E_c vs. T [60Wak1].

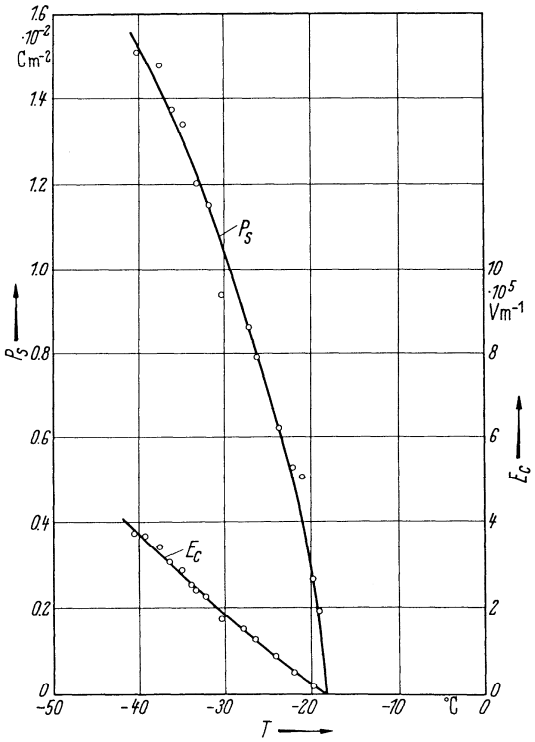

Fig. 48A-2-010. $K_4Fe(CN)_6 \cdot 3H_2O$. P_s, E_c vs. T near Θ [60Wak2].

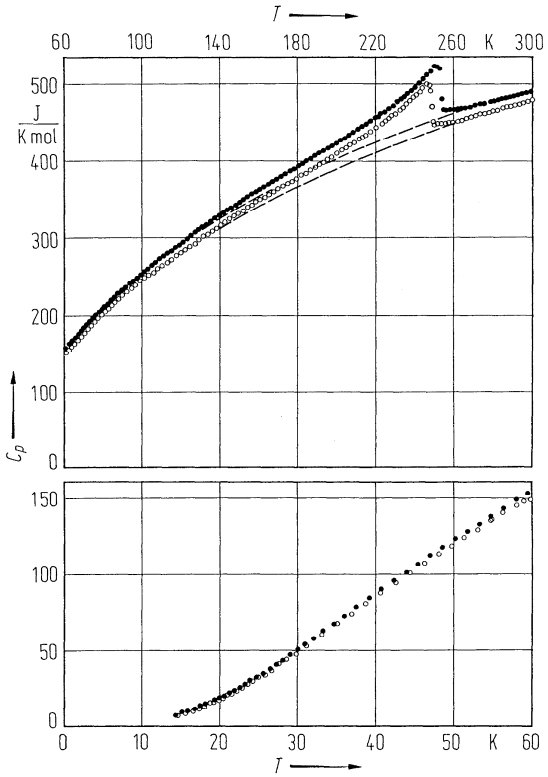

Fig. 48A-2-011. $K_4Fe(CN)_6 \cdot 3H_2O$, $K_4Fe(CN)_6 \cdot 3D_2O$. C_p vs. T [75Ogu]. Open circles: $K_4Fe(CN)_6 \cdot 3H_2O$; full circles: $K_4Fe(CN)_6 \cdot 3D_2O$. C_p: molar heat capacity at constant pressure.

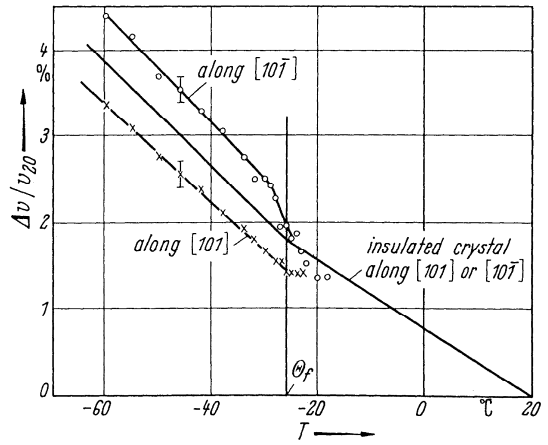

Fig. 48A-2-012. $K_4Fe(CN)_6 \cdot 3H_2O$. $\Delta v/v_{20}$ vs. T [67Sch]. $\Delta v/v_{20}$: percent change of sound velocity from that at 20 °C.

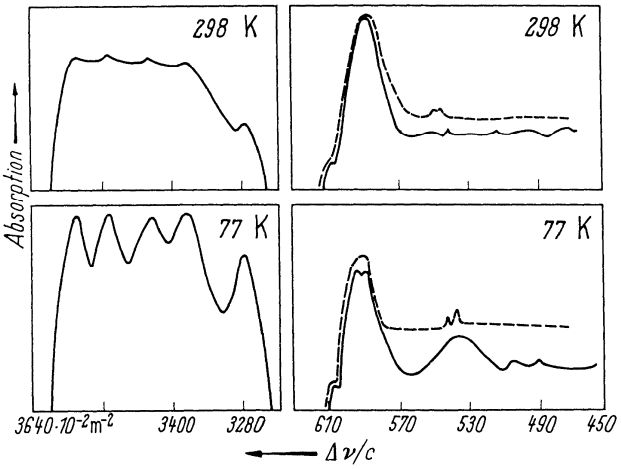

Fig. 48A-2-013. $K_4Fe(CN)_6 \cdot 3H_2O$. Infrared absorption vs. $\Delta\nu/c$ [61Bli]. Dashed line is for $K_4Fe(CN)_6$.

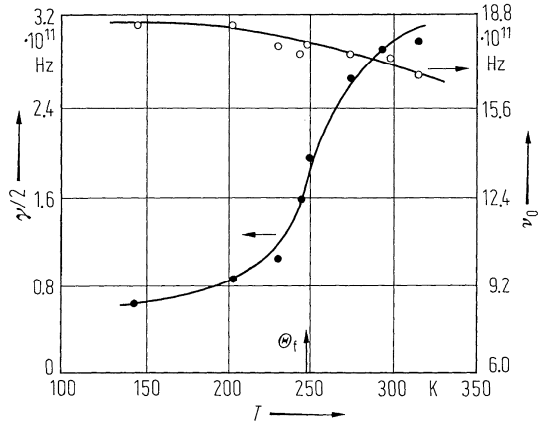

Fig. 48A-2-014. $K_4Fe(CN)_6 \cdot 3H_2O$. ν_0, $\gamma/2$ vs. T [77Sav1]. ν_0: characteristic frequency. γ: damping constant obtained from Raman scattering measurement [geometry $Y(ZY)Z$].

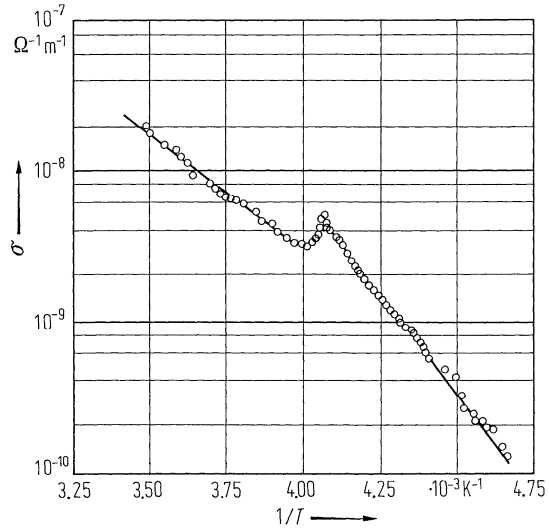

Fig. 48A-2-015. $K_4Fe(CN)_6 \cdot 3H_2O$. σ vs. $1/T$ [72Amo]. Ferroelectric $(10\bar{1})$ section.

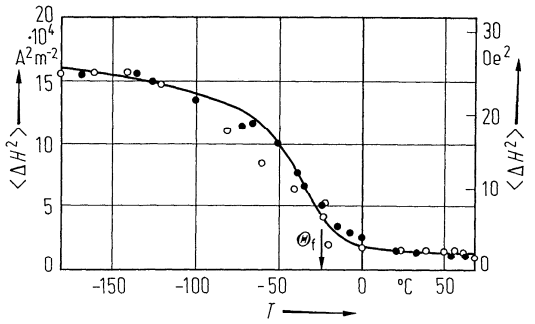

Fig. 48A-2-016. $K_4Fe(CN)_6 \cdot 3H_2O$. $\langle \Delta H^2 \rangle$ vs. T. Full circles: [64Kir]; open circles: [61Lun]. $\langle \Delta H^2 \rangle$: second moment of NMR of proton.

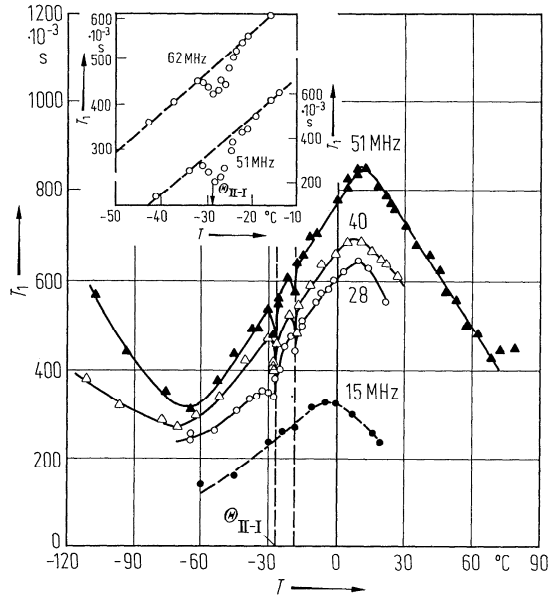

Fig. 48A-2-017. $K_4Fe(CN)_6 \cdot 3H_2O$. T_1 vs. T [74Bli]. Parameter: ν_H. T_1: proton spin-lattice relaxation time. ν_H: frequency of ac magnetic field.

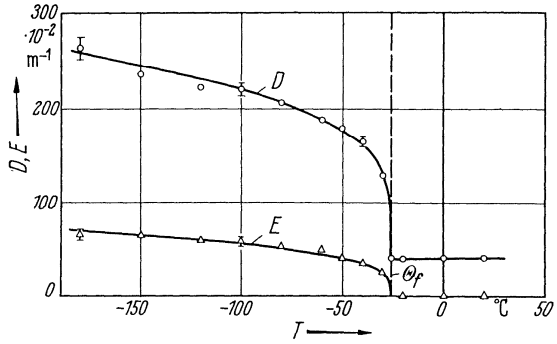

Fig. 48A-2-018. $K_4Fe(CN)_6 \cdot 3H_2O$. D, E vs. T [65ORe]. D, E: fine structure parameters in ESR.

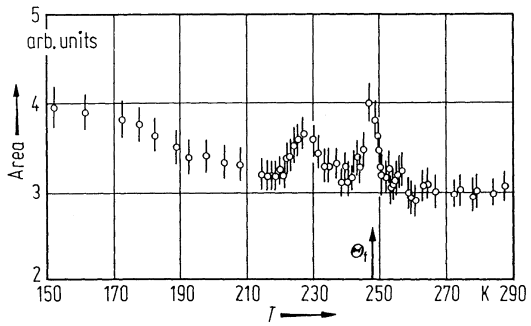

Fig. 48A-2-019. $K_4Fe(CN)_6 \cdot 3H_2O$. Area of the Mössbauer absorption line vs. T in the $[10\bar{1}]$ direction [71Mon].

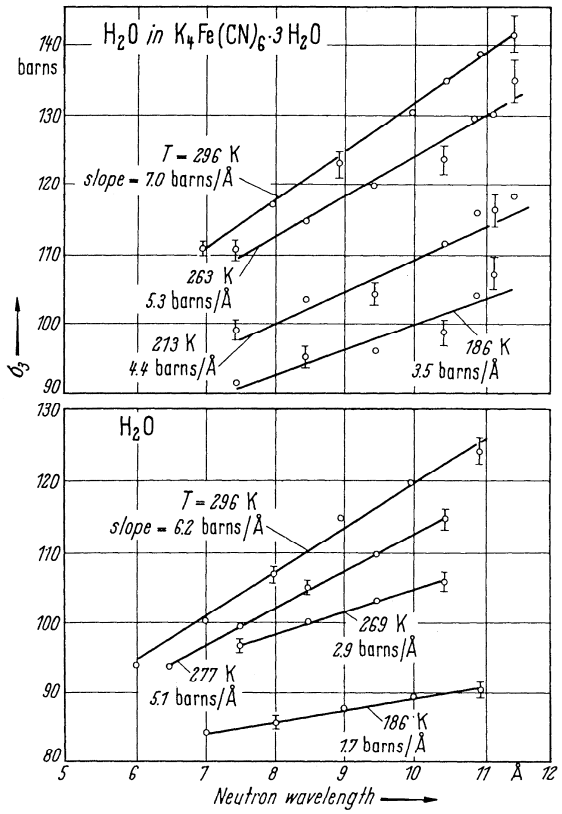

Fig. 48A-2-020. $K_4Fe(CN)_6 \cdot 3H_2O$. σ_3 vs. neutron wavelength [66Rus]. Parameter: T. σ_3: total scattering cross sections per hydrogen compared with scattering in water.